Ricci Flow for 3D Shape Analysis

Xianfeng Gu[1] Sen Wang[1] Junho Kim[1] Yun Zeng[1] Yang Wang[2] Hong Qin[1] Dimitris Samaras[1]

[1]Stony Brook University
[2]Carnegie Mellon University

Abstract

Ricci flow is a powerful curvature flow method in geometric analysis. This work is the first application of surface Ricci flow in computer vision. We show that previous methods based on conformal geometries, such as harmonic maps and least-square conformal maps, which can only handle 3D shapes with simple topology are subsumed by our Ricci flow based method which can handle surfaces with arbitrary topology. Because the Ricci flow method is intrinsic and depends on the surface metric only, it is invariant to rigid motion, scaling, and isometric and conformal deformations. The solution to Ricci flow is unique and its computation is robust to noise. Our Ricci flow based method can convert all 3D problems into 2D domains and offers a general framework for 3D surface analysis. Large non-rigid deformations can be registered with feature constraints, hence we introduce a method that constrains Ricci flow computation using feature points and feature curves. Finally, we demonstrate the applicability of this intrinsic shape representation through standard shape analysis problems, such as 3D shape matching and registration.

1. Introduction

Ricci flow is a powerful curvature flow method in Riemannian geometry. In particular, 3-manifold Ricci flow has been successfully applied to prove the Poincaré conjecture recently [21]. In this work, we introduce Ricci flow as a novel 3D shape representation for computer vision applications. We are motivated by the fact that Ricci flow can handle arbitrary topologies, allowing the mapping of any 3D surface to a 2D domain and its ability to handle large 3D shape deformation.

In recent decades, there has been a lot of research into surface representations for 3D surface analysis, which is a fundamental issue for many computer vision applications, such as 3D shape registration, partial scan alignment, 3D object recognition, and classification [4, 31, 22, 14]. In particular, as 3D scanning technologies improve, large databases of 3D scans require automated methods for matching and registration. However, matching surfaces undergoing non-rigid deformation is still a challenging problem, especially when data is noisy and with complicated topology. Different approaches include curvature-based representations [27], regional point representations [22, 25], spherical harmonic representations [7, 8], shape distributions [20], harmonic and conformal shape images [33, 28, 29], physics-based deformable models [26], Free-Form Deformation (FFD) [13], and Level-Set based methods [17]. However, many surface representations that use local shape signatures are not stable and cannot perform well in the presence of non-rigid deformation. Conformal geometric maps have been used in several applications of computer vision and graphics [33, 30, 9, 29, 15, 24, 28]. However, conventional conformal geometric methods can only handle surfaces with simple topologies or compute simple maps. As a result, most existing algorithms are limited to surfaces with simple topology such as genus zero with/without a single boundary. In contrast, our method can handle surfaces with *arbitrary* topologies for shape analysis.

The first contribution of this paper is to introduce a new 3D non-rigid surface analysis framework based on Ricci flow conformal mapping. Surface Ricci flow offers a novel means to manipulate shapes by curvatures and Riemannian metrics. With surface Ricci flow, the curvature evolves like a heat diffusion process on the surface and converges exponentially fast to a constant value. During the whole process, the angle structure on the surface is preserved, and the final surface can be embedded in one of the canonical domains, such as the sphere, the plane, or the hyperbolic space. By computing conformal maps using the Ricci flow method, each 3D surface, even with a complicated topology (e.g. having multiple holes), can be mapped to a 2D domain through a global optimization. The resulting map does not have any singularities and is a diffeomorphism, i.e., *one-to-one* and *onto*. These maps are stable, insensitive to resolution changes, and robust to noise. Hence, the original 3D surface-matching problem simplifies to a 2D image-matching problem of the conformal geometric maps, which is a better understood problem [16, 2, 19].

Our second contribution is to show that the previous conformal map methods are subsumed by Ricci flow. Hence, our framework is more general, while we can take advantage of the significant body of work for 3D surface analysis using previous conformal map methods [33, 24, 9, 30, 29, 28].

Our final contribution is to integrate feature constraints in Ricci flow computation. Taking advantage of meaningful features is essential for any matching or registration method. In the case of large non-rigid deformations, matched features allow accurate description of the deformations. Thus, in order to make Ricci flow applicable to computer vision problems, we develop: i) a representation of feature points and feature curves suitable to our framework; ii) a novel feature based metric; iii) an algorithm which, based on features, decomposes the surface into conformal patches; and iv) an algorithm to embed these patches onto the plane. On the target canonical domains, the entire curvature is concentrated on feature points; feature curves are mapped to straight boundary lines. This association of feature points with target domain curvature is novel and has broader implications for geometric modeling and graphics.

Finally, we provide initial experiments that demonstrate the potential of our method in a broad range of 3D shape analysis applications such as 3D shape matching and registration in a variety of data sets including face scans and biomedical data.

The rest of the paper is organized as follows: The mathematical background of the Ricci flow conformal maps is introduced in Section 2. Discrete Ricci flow is explained in Section 3. A framework for 3D surface representation and matching using Ricci flow is proposed in Section 4 and 5. Experimental results are presented in Section 6, and we conclude with discussion and future work in Section 7.

2. Theoretical Background

This section briefly introduces the theoretic background of surface Ricci flow. (For details, see [12].)

Let S be a smooth surface embedded in $\mathbb{R}^3$, then S has an induced Euclidean metric $\mathbf{g}$. Suppose $u : S \to \mathbb{R}$ is a function on the surface, we can define another metric $\bar{\mathbf{g}} = e^u\mathbf{g}$, which is *conformal* to the original metric $\mathbf{g}$ with an area distortion factor e^{2u}. We call u the *conformal factor*.

Furthermore, when the metric of S is changed from $\mathbf{g}$ to $\bar{\mathbf{g}}$ along the change of u, every intrinsic property (e.g., Gaussian and geodesic curvatures) of S is changed. The Gaussian curvature k of interior points changes by $\bar{k} = e^{-2u}(k - \Delta u)$, where Δ is the Laplace-Beltrami operator [5] induced by the original metric $\mathbf{g}$. The geodesic curvature k_g on the boundary points changes as $\bar{k}_g = e^{-u}(k_g - \frac{\partial u}{\partial \mathbf{n}})$, where $\mathbf{n}$ is the normal to the boundary of the surface ∂S.

Although the curvature value at a point is determined from the Riemannian metric, the sum of the total curvatures solely depends on the topology of the surface, as described in the Gauss-Bonnet formulae [5], such that $\int_S kdA + \int_{\partial S} k_g ds = \int_S \bar{k}d\bar{A} + \int_{\partial S} \bar{k}_g d\bar{s} = 2\pi\chi(S)$, where $\chi(S)$ is the Euler characteristic number of the surface S.

S	Surface
$\mathbf{g}$	original Riemannian metric
$\bar{\mathbf{g}}$	target Riemannian metric conformal to the original one
u	Conformal factor
$k, \bar{k}$	original and target Gaussian curvatures under $\mathbf{g}$ and $\bar{\mathbf{g}}$, resp.
$k_g, \bar{k}_g$	original and target geodesic curvatures under $\mathbf{g}$ and $\bar{\mathbf{g}}$, resp.
χ	Euler number
$dA_{\mathbf{g}}$	the area element under $\mathbf{g}$
M	triangular mesh
v_i	the i-th vertex
e_{ij}	the edge connecting v_i, v_j
f_{ijk}	the face formed by v_i, v_j and v_k
l_{ij}	edge length of e_{ij}
ϕ_{ij}	the intersection angle between circles centered at v_i and v_j
γ_i	radius of the circle at vertex v_i
k_i	discrete vertex curvature of v_i
Δ	Laplace-Beltrami operator
w_{ij}	edge weight
τ	A conformal map from the surface to the plane
ϕ	A map between two surfaces
$\bar{\phi}$	A map between two conformal domains

Table 1. Symbol list

Ricci flow is a powerful tool to compute the desired metric $\bar{\mathbf{g}}$ which satisfies the given target curvature $\bar{k}$, from the induced metric $\mathbf{g}$ in S. Suppose S is a closed surface with a Riemannian metric $\mathbf{g}$, the Ricci flow is defined as

$$\frac{d\mathbf{g}}{dt} = -2k\mathbf{g}, \tag{1}$$

where k is the Gaussian curvature determined by the current metric.

Surface Ricci flow deforms a Riemannian metric $\mathbf{g}$ to another metric $e^{2u(t)}\mathbf{g}$, which is conformal to the original one. When the desired target curvature $\bar{k}$ is given, then the corresponding conformal metric can be achieved by the following general Ricci flow $\frac{du(t)}{dt} = 2(\bar{k} - k(t))$. Eventually, the limit metric $\mathbf{g}(\infty)$ becomes $\bar{\mathbf{g}}$, which is conformal to $\mathbf{g}$ and satisfies the target curvature $\bar{k}$.

3. Generalization of Conformal Maps

Conventional conformal geometric methods, such as harmonic maps, least squares conformal maps (LSCMs), and methods based on holomorphic forms, can be unified by Ricci flow. In order to clarify this point, we first compare Ricci flow with conventional methods. Then, we briefly introduce the discrete Ricci flow and show the intrinsic connection between Ricci flow and other conformal geometric maps such as harmonic maps.

3.1. Comparing with conventional conformal map methods

In general, conformal mapping algorithms can be classified to the following categories. The first class computes

maps from the surface to the plane, such as harmonic maps [30, 33], least squares conformal maps (LSCMs) [28, 15], spherical conformal maps [1, 9]; The second class aims at computing the derivatives of maps, such as the method based on holomorphic forms [10]; The third class computes the conformal metrics to induce conformal maps. The Ricci flow method belongs to the third class, which is more general than the other two classes.

A conformal map induces a pull-back metric on the surface which induces zero Gaussian curvature on the surface. Conversely, the map can be recovered by its pull-back metric directly. Since the curvature is zero everywhere in the map, the pull-back metric can be computed using Ricci flow by specifying the target curvature 0 everywhere. Therefore, any conformal maps (with zero target curvature) which can be computed using harmonic maps, LSCMs or holomorphic 1-form methods can be computed by Ricci flow.

The main difference between Ricci flow and conventional methods is in how complicated are the topologies they can handle. In particular, the algorithms in the first class can handle surfaces with genus 0 with/without a single boundary, but can not handle high genus cases. The algorithms in the second class can handle all topologies, but they can not compute the conformal maps between multi-holed annuli, as shown in Fig. 5, which are frequently encountered in the scanning process. Furthermore, if the target surface has arbitrary curvature, only Ricci flow can find the map. Therefore, Ricci flow is much more general, and all algorithms in the other two categories can only handle a subset of the problems handled by Ricci flow [1].

Ricci flow can address situations that can not be handled by other existing algorithms, such as Iterative Closest Point (ICP) [23] and level set based methods [17]. ICP can find a good rigid alignment in $\mathbb{R}^3$, but for non-rigid surface deformations, such as the bending deformation shown in Fig. 3, ICP can not find a good registration between two surfaces. Level set based methods are powerful tools for surface analysis. However, it is required that the surface deformation process performed explicitly in $\mathbb{R}^3$ at each step, which will be difficult for surfaces with complex topology since the deformed surface may not be able to be embedded in $\mathbb{R}^3$.

3.2. Discrete Ricci flow

Conventional Ricci flow is defined on C^2 smooth surfaces. In this section, we focus on the discrete approximation of Ricci flows on triangular meshes [6], which is robust for polygonal meshes with sharp corners. Discrete Ricci flow is useful for handling noisy data sets in real applications, as shown in the heart registration example in Sec. 6.

The key observation about the discrete Ricci flow is that the conformal metric deformation can be treated as a

[1]A formal proof based on Riemann surface theory is provided in http://www.cs.sunysb.edu/∼manifold/iccv07/suppl.pdf

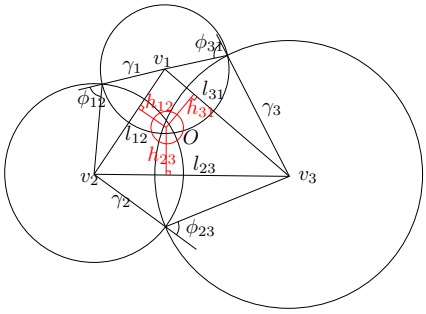

Figure 1. Circle packing metric for a triangle. The dual circle (the red one) in orthogonal to the other 3 circles.

local scaling transformation, which preserves angles and transforms an infinitesimal circle to an infinitesimal circle. Therefore, the general idea of the discrete Ricci flow is to cover the mesh by many circles centered at the vertices. Each circle has a cone angle at the vertex, which can be treated as the discrete curvature. Then, by adjusting the circle radii, we can deform the Riemannian metric of the mesh in a discrete conformal way [6]. The change of the circle radii is the analogy to the change of the conformal factor u. The relation between the discrete curvature and the discrete conformal factor is *exactly the same* as that in the smooth case.

Suppose M is a mesh with boundary ∂M. A circle packing metric (M, Γ, Φ) for M is shown in Fig.1, where Γ and Φ represent the radius function of circles on each vertex and the intersection angle between two circles at each edge, respectively. Each edge length is determined by using the cosine law with the radii of two circles and the intersection angle on the edge. The vertex curvature $k(v)$ measures the flatness of its neighborhood, which is defined as $2\pi - \sum_i \alpha_i$ for an interior vertex and $\pi - \sum_i \alpha_i$ for a boundary vertex, where α_i's are the corner angles surrounding a vertex v. As in the smooth case, the discrete version of the Gauss-Bonnet formulae holds, $\sum_v k(v) = 2\pi\chi(M)$. Two circle packing metrics (M, Γ_1, Φ_1) and (M, Γ_2, Φ_2) are conformal, if and only if $\Phi_1 \equiv \Phi_2$.

Therefore, the discrete Ricci flow can be defined in the similar way to Eq. 1 as $\frac{d\gamma_i(t)}{dt} = -2k_i\gamma_i(t)$, which converges to constant curvature under the constraint that the total area of the mesh is fixed. If we define the *discrete conformal factor* as $\mathbf{u} = \{\ln\gamma_1, \ln\gamma_2, \cdots, \ln\gamma_n\}$ and the prescribed target curvature as $\bar{\mathbf{k}} = \{\bar{k}_1, \bar{k}_2, \cdots, \bar{k}_n\}$, then the general discrete Ricci flow is $\frac{du_i(t)}{dt} = \bar{k}_i - k_i(t)$, which will lead to the desired conformal metric satisfying the desired target curvature.

In fact, Ricci flow is the gradient flow of a specific energy form, *Ricci energy*, $E(\mathbf{u}) = \sum_i (\bar{k}_i - k_i)du_i$. Ricci energy is convex [6], and therefore it has a unique global optima $\bar{\mathbf{u}}$, which induces the target curvature $\bar{\mathbf{k}}$. In practice, optimizing Ricci energy is more efficient than computing Ricci flow. The convex Ricci energy can be stably opti-

mized using Newton's method. The Hessian matrix of the energy $E(\mathbf{u})$ can be computed explicitly as follows.

Suppose $f_{ijk} \in F$ is a face on the mesh, there exists a unique circle orthogonal to all three circles at the vertices, shown as the red circle in Fig. 1. We denote the center of that circle as o_{ijk}. The distance from o_{ijk} to the edge e_{ij} is denoted as h_{ij}^k. If an interior edge $e_{ij} \notin \partial M$ is shared by two faces f_{ijk} and f_{jkl}, its weight is $w_{ij} = h_{ij}^k + h_{ji}^l$. If the edge is on the boundary, and only adjacent to face f_{ijk}, its weight is $w_{ij} = h_{ij}^k$.

The Hessian matrix of $E(\mathbf{u})$ has the following formulae:

$$\frac{\partial^2 E(\mathbf{u})}{\partial u_i \partial u_j} = \begin{cases} -w_{ij} & i \neq j, e_{ij} \in E \\ \sum_k w_{ik} & i = j, e_{ik} \in E \\ 0 & otherwise \end{cases},$$

which is positive definite on the hyperplane $\sum u_i = const$.

Now, we will describe how to obtain the conformal map of a given surface from the conformal metric obtained from Ricci flow. Alg. 1 shows the procedures of computing the desired conformal metric by prescribed curvature by minimizing the Ricci energy. For surfaces with boundaries, we introduce a novel metric computed by Alg. 2, such that all interior points have zero curvature, and the vertices on the same boundary component share the same curvature. Intuitively, this metric will flatten the surface and map all the boundaries to circles, as shown in Fig. 3.

Algorithm 1 Compute Conformal Metric by Prescribed Curvature Using Ricci Flow

while $|\bar{\mathbf{k}} - \mathbf{k}| > \epsilon$ **do**
  Compute dual circles
  Compute edge weight w_{ij}
  Form the Hessian matrix $\Delta(\mathbf{u})$
  Solve $\Delta(\mathbf{u})d\mathbf{u} = (\bar{\mathbf{k}} - \mathbf{k})$ constrained at $\sum_i du_i = 0$
  Update $\mathbf{u} = \mathbf{u} + d\mathbf{u}$
  Update $\mathbf{k}$
end while

Algorithm 2 Compute Uniform Flat Metric

Compute the boundary components, $\partial M = C_1 \cup C_2 \cup \cdots \cup C_k$.
$\forall v \notin \partial M$, set $\bar{k} \Leftarrow 0$.
$\forall v \in C_j$, $\bar{k}(v) \Leftarrow s_j \frac{2\pi}{|C_j|}$, where $s_1 = 1$, $s_j = -1$ for $j \neq 1$.
while $|\bar{\mathbf{k}} - \mathbf{k}| > \epsilon$ **do**
  Compute $\bar{\mathbf{u}}$ by $\bar{\mathbf{k}}$ using the Ricci energy algorithm.
  $\forall v \in C_j$, $\bar{k}(v) \Leftarrow \frac{s_j \pi (\bar{l}(e_-) + \bar{l}(e_+))}{\sum_{e \in C_j} \bar{l}(e)}$,
  where $\bar{l}(e)$ is the edge length under $\bar{u}$, and
  e_- and e_+ represent two boundary edges incident to v.
end while

Once the metric is obtained, the mesh can be isometrically embedded onto the plane. The isometric embedding is denoted as $\tau : V \to \mathbb{C}$. This embedding in fact is harmonic, namely, it minimizes the harmonic energy $E(\tau) = \sum_{e_{ij} \in E} w_{ij} |\tau(v_i) - \tau(v_j)|^2$, i.e., $\Delta(\mathbf{u})\tau = 0$. The formal proof will be given in an extended version of this work.

4. Feature Based Canonical Domain Decomposition

In practice, it is often useful to add feature constraints, such as point and curve correspondences when comparing 3D shapes. Hence we propose the incorporation of such constraints to the energy minimization and formulate the main framework of surface matching using Ricci flow in the following commutative diagram,

$$\begin{array}{ccc} S_1 & \xrightarrow{\phi} & S_2 \\ {\scriptstyle \tau_1}\downarrow & & \downarrow{\scriptstyle \tau_2} \\ D_1 & \xrightarrow{\bar{\phi}} & D_2 \end{array}$$

S_1, S_2 are two given surfaces, $\phi : S_1 \to S_2$ is the desired matching. We use Ricci flow to compute $\tau_i : S_i \to D_i$ which maps S_i conformally onto the canonical domain D_i. D_1 and D_2 can also be surfaces other than simple planar domains. The topology and the curvature of D_1 and D_2 incorporate the major feature information of the original surfaces S_1 and S_2. If there are certain feature constraints, we can further incorporate them using the method described below and compute a map $\bar{\phi} : D_1 \to D_2$. The final map ϕ is induced by $\phi = \tau_2^{-1} \circ \bar{\phi} \circ \tau_1$.

For surfaces with significant point features, we design the target curvature such that those features are transformed to the branch points of the Riemann surfaces in the target domains. Alg. 3 uses features to design such target domains.

After computing the metric incorporating all the major features using Alg. 4, the surface is decomposed to canonical patches. As described in Sec. 3.2, each patch is embedded onto the plane by minimizing the harmonic energy with the feature point position constraints as described in Alg. 5.

An example result on a scanned human face is demonstrated in Fig. 2. The original surface is a 2-holed annulus. We select the nose tip as the only feature point, and set the target curvature to be zero everywhere (including both the interior points and the boundary points) except for the noise tip, whose curvature equals to -2π. Then, we use Ricci flow to compute the target metric of the Riemann surface, which is a flat surface with a single branch point. Because the target surface can not be embedded in $\mathbb{R}^3$ directly, we decompose it to canonical patches. The decomposition includes three steps: First, under the target metric we find straight lines from the branch point to the boundaries, each of which is perpendicular to a boundary. Next, we trace the straight lines which are parallel to the boundaries under the target metric. Finally, all the straight lines partition

the surface to patches and each patch is conformally embedded onto the plane either as a rectangle or a trapezoid (see Fig. 2). Thanks to the conformal deformation, this decomposition is solely determined by the geometry of the original surface and the choice of features. Therefore, surface matching and registration can be carried out by matching the decomposed patches on the planar domain, while the features are guaranteed to match as they become patch corners or boundaries.

Algorithm 3 Computing Feature Based Flat Metric

Specify the feature curves
Slice the surface open along the feature curves.
Specify the feature points $\{v_1, v_2, \cdots, v_m\}$.
Compute the boundary components, $\partial M = C_1 \cup C_2 \cup \cdots \cup C_k$.
for each vertex $v \in M$, set $\bar{k} \Leftarrow 0$.
Allocate curvature on feature points, $\bar{k}_i = 2m_i\pi, m_i \in \mathcal{Z}$, $\sum_i m_i = \chi(M)$.
Use Ricci energy optimization to compute the metric.

Algorithm 4 Computing Feature Based Domain Decomposition

Compute the feature based target metric, such that all boundaries become straight lines under the target metric.
Compute the straight lines starting from the feature points which are perpendicular to the boundaries under the new metric.
Compute the straight lines parallel to boundaries under the new metric.
Slice the surface open along the straight lines to decompose the surface to patches, each of which is conformally mapped to a rectangle or a trapezoid.

Algorithm 5 Computing the Isometric Embedding

On each face, compute the dual circle which is orthogonal to all three vertex circles.
Compute the distance from the center of the dual circle to three edges.
Embed a seed triangle f on the mesh.
Minimize the harmonic energy with the constraints of the embedded triangle f.

The main reason for the decomposition is to improve the efficiency and accuracy of the method. We convert surface matching to the simpler processes of matching between rectangles and trapezoids. Because we incorporate feature constraints to the mapping by minimizing harmonic energy, which requires the domain to be convex, the decomposition is also necessary to ensure the convexity and to guarantee the globally optimal solution.

5. Ricci Flow Based Shape Representation

In this section, we present a new shape representation for 3D surface analysis, such as shape matching and registration based on Ricci flow, which can handle surfaces with

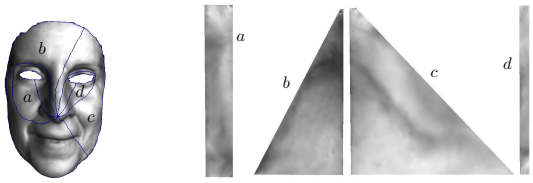

(a) A face surface with segmenting curves (b) Planar domain for each patch

Figure 2. Canonical surface decomposition using Ricci flow. The nose tip is selected as a feature point. A flat metric is computed using Ricci flow, such that all interior points and all boundary points are with zero curvatures, except for the feature point where the Gaussian curvature equals to -2π. Straight lines under the new metric, which are either parallel or perpendicular to the boundaries, result in the blue curves on the original surface that pass through the feature point in (a). Then the surface is decomposed to patches, each patch is conformally equivalent to a rectangle or a trapezoid on the plane, shown in (b).

varying boundaries and arbitrary topologies. Moreover, it also allows multiple types of feature constraints, such as feature point constraints, feature curve constraints, and target curvature constraints. Therefore, it provides a unified framework for non-rigid 3D surface analysis.

Ricci Flow Shape and Texture Images The main advantage of the Ricci flow method is that it can convert all 3D problems into 2D domains. By computing conformal maps using the Ricci flow method, each 3D surface, even with a complicated topology (e.g. having multiple holes) can be mapped to a 2D domain through a global optimization. Therefore, we can generate the Ricci flow shape images by associating a shape attribute with each vertex in the Ricci flow conformal maps. Among the shape attributes, we use mean curvatures to obtain Ricci flow conformal images since mean curvature depends only on surface geometry. In our method, the mean curvature is computed in the same way as in [9]. Moreover, it is also possible to generate other Ricci flow conformal images by associating other attributes such as textures.

Surface Matching with Ricci Flow Representation Given two general surfaces S_1 and S_2, we first compute the Ricci flow shape or texture images. Because the resulting maps do not have any singularities and are a diffeomorphism, i.e., one-to-one and onto, we can register these two 3D surfaces by simply matching and registering with the aligned Ricci flow shape or texture images. We evaluate the accuracy of surface matching by using the error distance between the two resulting maps, as follows.

$$normalized\ error_{S_1,S_2} = \frac{\sum_{i=1}^{N} \|p_i^{S_1} - p_i^{S_2}\|}{\sum_{i=1}^{N} \|p_i^{S_1}\|} \quad (2)$$

where N is the number of overlapping points in the Ricci flow conformal shape or texture images of 3D surface S_1

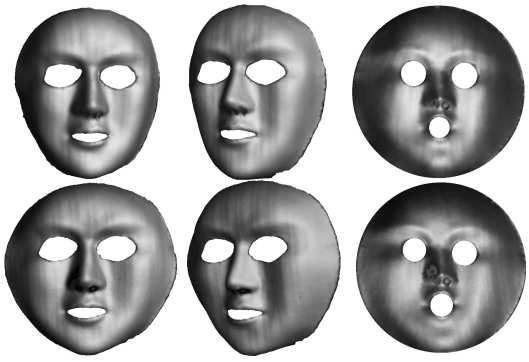

Figure 3. Surface matching under isometric deformation using a toy mask. The first row shows two views of the original surface and its conformal image; the second row shows two views of the deformed surface and its conformal image. Pixel intensities in the conformal images are copied from the corresponding points in the 3D scans. Under isometric deformation, the conformal images are identical. The normalized registration error is 0.0177 computed using Eq. 2.

and S_2, and $p_i^{S_k}$ is the value of point i in the 2D image of surface $S_k (k = 1, 2)$. This is the matching method used in our experiments.

6. Experimental Results

In this section, we demonstrate the performance of our framework by several experiments on real 3D data, such as isometrically deformed surfaces, dynamic facial expression with complex topology, and human heart surfaces undergoing complex non-rigid motion deformations.

Isometrically deformed surfaces First, as a simple experiment, we test our method on isometrically deforming data. We scanned a flexible (but non-stretchable) toy mask two times, once for the original and again for its deformed version. Since there is no stretching, the deformation is isometric and can be easily handled by Ricci flow. The conformal images of the two scans are practically identical with normalized error 0.0177.

6.1. Experiments on complex topology

As described in Sec. 3, the major advantage of our method compared to the existing 3D surface-matching methods based on conformal geometric maps [28, 15, 30, 33] is that our framework can handle surfaces with arbitrary topology directly. Therefore, for surfaces with multiple holes our method does not require additional pre-processing steps such as hole fillings. Fig. 4 shows a comparison between our method and the LSCM-based method [28] and the harmonic map based methods [30]. Fig. 4 (a, f) show the original 3D surfaces of the same subject with different expressions, and Fig. 4 (b, g) depict the resulting Ricci flow texture images computed by our method. Since the LSCM-based method and harmonic maps can only handle disk topology, the holes in the eye and mouth on the original 3D scan data need to be filled before computing the 2D conformal map, as shown in Fig. 4(c, h). As shown in Fig. 4(d, i) and Fig. 4(e, j), the introduction of fake geometry to fill the holes leads to large distortion errors around the eye and mouth areas in both least-squares conformal maps and harmonic maps. Notice that our texture images obtained from Ricci flow have no signification distortions as shown in Fig. 4 (b, g), although we leave the holes as they are in the raw data.

The normalized matching error of Ricci flow is 0.0584, compared to 0.0723 for LSCM and 0.0814 for harmonic maps. All errors were computed using Eq. 2, where hole areas were not included. Our method is robust enough to handle limited amounts of non-isometric deformations (which violate the Ricci flow definition). However, large deformations can be handled with the incorporation of feature constraints as described in the following experiment.

6.2. Matching dynamic non-rigid 3D data

In order to demonstrate the performance of our method on dynamic non-rigid surfaces, we captured 3D facial expression data using a phase-shifting structured light ranging system [34] at 30 frames per second. Since our method allows feature curve correspondence constraints, we detect the contours of the lips and the eyes and integrate them into the computation of the Ricci flow maps (these curves can be detected by methods such as [32, 18]). Based on the resulting 2D maps, we can perform the registration between two scanned faces with different expressions, as shown in Fig. 5. Since the deformation between two scanned faces is non-rigid, the surface matching with single maps is problematic as shown in the 2nd column in Fig. 5. In this case, we apply the decomposition method described in Sec. 4. The 3rd-5th columns in Fig. 5 illustrate the pairs of the Ricci flow images which correspond to the parts of the original surfaces as shown in the 1st column in Fig. 5 [2]. Each pair of patches is registered with the corresponding patch boundaries, and we measure the errors between the patches by Eq. 2.

The original registration error between two faces in Fig. 5 is 0.0447. In order to demonstrate the robustness of the feature detection accuracy in our decomposition method, we randomly perturb the feature point around the nose tips in Fig. 5. The average error of three different perturbations within a 3mm (resp. 6mm) radius is 0.045 (resp. 0.048).

Although our method is not limited to face data, it is interesting to compare our method with the face registration method based on multi-dimensional scaling [3]. Compared to the method of Bronstein et al. [3], which is not guaranteed to obtain global optima in isometric embedding, our method reaches global optima in handling anisometric data with arbitrary topologies, as shown int the following heart experiments.

[2] A video of the decomposition is available at http://www.cs.sunysb.edu/∼manifold/iccv07/video.avi

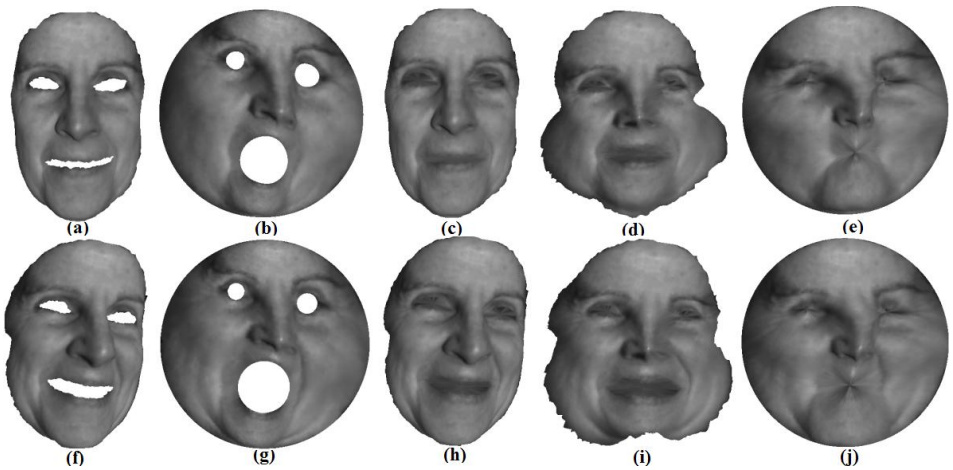

Figure 4. Comparison of Ricci flow with LSCM and harmonic maps. (a) and (f) are two surfaces to be registered. (b) and (g) are their Ricci flow maps. (c) and (h) are these two surfaces after hole-filling. (d) and (i) are their LSCMs. (e) and (j) are their harmonic maps. The registration error of Ricci flow using Eq. 2 is 0.0584, while, the registration errors (without including the area of holes) of LSCMs and harmonic maps are 0.0723 and 0.0814, respectively.

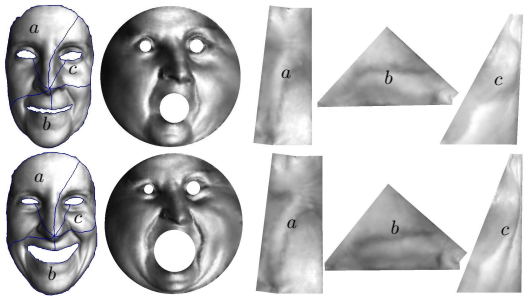

Figure 5. Registration of facial expression data using feature based domain decomposition. The first column shows two face scans with large deformation. The second column shows the planar domains computed using uniform flat metrics. Because of the large deformation, there is significant difference between the planar domains. Selecting the nose tip as the feature point, the surfaces are decomposed to canonical planar domains using the method described in Sec. 4. The surfaces are registered by matching the corresponding planar domains.

In the biomedical domain, we experimented with a deforming heart sequence. The original tagged data were acquired using a 3T MRI machine. The data are image sequences from end diastole to end systole. The reconstruction was done based on methods developed by the authors of [11], who made the data available to us. The output from the analyzed data result are 3D corresponding points over time from end disatole to end systole. We experimented using a sequence of 21 frames of 3D corresponding points. Experiments were performed on the deforming 3D surface. The given 3D correspondences were not used in the experiments, but only as ground truth.

In order to test the robustness of our method to initial surface segmentation, we experiment using only the left ventricle data. We first detect and segment along the boundary between the surface of the left ventricle and the rest of the heart. After segmenting the heart data for each frame, we apply the Ricci flow algorithm to map each heart into its canonical planar domain, and register each adjacent frame by mapping the corresponding planar domains. In a first experiment, we manually defined a boundary on the first frame and consistently kept these points as the boundary points throughout the sequence. Even though there are large interior deformations, the boundary is sufficient in establishing almost perfect surface correspondences, with an average registration error of 0.006197. In the second experiment, the boundary was automatically determined based on curvature, using the VTK software package. These boundary points are not guaranteed to be consistent across frames. The method is still very robust with an average registration error of 0.030331.

Fig. 6 illustrates the effectiveness of registration using Ricci flow. The first frame is texture-mapped with a grid pattern both in the experimental and ground truth data, in order to better visualize the deformation. Although the non-rigid deformation of the heart is significant between different frames, our method captures the deformation almost indistinguishably from the ground truth.

7. Conclusion and future work

This paper proposed a 3D shape analysis method based on surface Ricci flow. Since Ricci flow is a powerful tool to handle geometries with arbitrary topologies our method can unify conventional methods based on conformal geometry. It also allows different types of feature constraints, such as feature point and curve constraints, to handle large deformations and to further improve the accuracy of surface matching and registration. A series of algorithms was introduced to map the 3D surfaces onto canonical 2D domains, and a new surface representation is proposed to combine multiple features for 3D shape analysis. Finally, the gener-

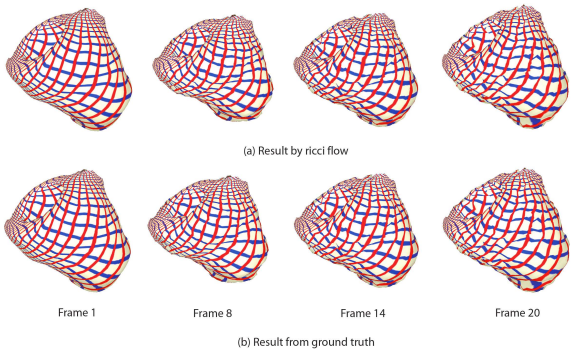

Figure 6. Registration of 3D dynamic heart data. Registration results using Ricci flow for 4 different frames are shown in the top row. The original heart data for the same frames are shown in the bottom row. The data on frame 1 were texture mapped with a grid pattern, that helps to visualize the subsequent non-rigid deformations.

ality and flexibility of Ricci flow were demonstrated by various experiments on human face scans and dynamic heart surface data. In future work, we will continue to explore properties of Ricci flow maps (to derive for example the optimal surface parameterization using Ricci flow) and to reduce computational complexity, especially when a large number of feature constraints are given. We also plan to use our framework for applications such as 3D object classification and recognition under non-rigid deformations.

Acknowledgements

The authors are grateful to Profs. Peisen Huang and Dimitri Metaxas for providing the face and heart data used in this paper. This work was partially supported by NFS Career awards CCF-0448339, CCR-9896123, NSF grants DMS-0528363, DMS-0626223, IIS-0527585, DMI-9896170, IIS-0082035, IIS-0097646, IIS-0527585, CNS-0627645, ACI-0313184, DOJ grant 2004-DD-BX-1224, GAANN grant P200A9703199, a Honda Initiation Award, an Alfred P. Sloan Fellowship, and the IITA&MIC scholarship program.

References

[1] S. Angenent, S. Haker, A. Tannenbaum, and R. Kikinis. On the laplace-beltrami operator and brain surface flattening. *IEEE Trans. Med. Img.*, 18(4):700–711, 1999.

[2] V. Athitsos, J. Alon, S. Sclaroff, and G. Kollios. Boostmap: a method for efficient approximate similarity rankings. *CVPR04*, II:268–275.

[3] A. Bronstein, M. Bronstein, and R. Kimmel. Three dimensional face recognition. *IJCV*, 64(1):5–30, 2005.

[4] R. Campbell and P. Flynn. A survey of free-form object representation and recognition techniques. *CVIU*, 81:166–210, 2001.

[5] M. D. Carmo. *Differential Geometry of Curves and Surfaces*. Prentice Hall, 1976.

[6] B. Chow and F. Luo. Combinatorial ricci flows on surfaces. *Journal Differential Geometry*, 63(1):97–129, 2003.

[7] A. Frome, D. Huber, R. Kolluri, T. Bulow, and J. Malik. Recognizing objects in range data using regional point descriptors. *ECCV04*, III:224–237.

[8] T. Funkhouser, P. Min, M. Kazhdan, J. Chen, A. Halderman, D. Dobkin, and D. Jacobs. A search engine for 3d models. *ACM TOG*, 22(1):83–105, 2003.

[9] X. Gu, Y. Wang, T. F. Chan, P. M. Thompson, and S.-T. Yau. Genus zero surface conformal mapping and its application to brain surface mapping. *IEEE Trans. Med. Img.*, 23(7), 2004.

[10] X. Gu and S.-T. Yau. Global conformal parameterization. *SGP 2003*, pages 127–137.

[11] E. Haber, D. N. Metaxas, and L. Axel. Motion analysis of the right ventricle from mri images. In *MICCAI '98*, pages 177–188.

[12] R. S. Hamilton. The ricci flow on surfaces. *Mathematics and general relativity*, 71:237–262, 1988.

[13] X. Huang, N. Paragios, and D. Metaxas. Establishing local correspondences towards compact representations of anatomical structures. *MICCAI03*, 2:926–934, 2003.

[14] D. Huber, A. Kapuria, R. Donamukkala, and M. Hebert. Parts-based 3d object classification. *CVPR04*, II:82–89.

[15] B. Levy, S. Petitjean, N. Ray, and J. Maillot. Least squares conformal maps for automatic texture atlas generation. *SIGGRAPH02*, pages 362–371.

[16] D. Lowe. Distinctive image features from scale-invariant keypoints. *IJCV*, 60(2):91–110, 2004.

[17] R. Malladi, J. A. Sethian, and B. C. Vemuri. A fast level set based algorithm for topology-independent shape modeling. *J. Math. Imaging and Vision*, 6(2/3):269–290, 1996.

[18] I. Matthews, T. Cootes, J. Bangham, S. Cox, and R. Harvey. Extraction of visual features for lipreading. *PAMI*, 24(2):198–213, 2002.

[19] G. Mori, S. Belongie, and J. Malik. Efficient shape matching using shape contexts. *PAMI*, 27(11):1832–1837, 2005.

[20] R. Osada, T. Funkhouser, B. Chazelle, and D. Dobkin. Shape distributions. *ACM TOG*, 21:807–832, 2002.

[21] G. Perelman. Finite extinction time for the solutions to the ricci flow on certain three-manifolds. Technical Report arXiv.org, July 17 2003.

[22] S. Ruiz-Correa, L. Shapiro, and M. Meila. A new paradigm for recognizing 3d object shapes from range data. *ICCV03*, II:1126–1133.

[23] S. Rusinkiewicz and M. Levoy. Efficient variants of the ICP algorithm. In *Proc. the 3rd Intl. Conf. on 3D Digital Imaging and Modeling*, pages 145–152, 2001.

[24] E. Sharon and D. Mumford. 2d-shape analysis using conformal mapping. *CVPR04*, II:350–357.

[25] Y. Sun and M. Abidi. Surface matching by 3d point's fingerprint. *ICCV01*, II:263–269.

[26] D. Terzopoulos, A. Witkin, and M. Kass. Constraints on deformable models: Recovering 3d shape and nonrigid motion. *Artificial Intelligence*, 35:91–123, 1988.

[27] B. Vemuri, A. Mitiche, and J. Aggarwal. Curvature-based representation of objects from range data. *IVC*, 4:107–114, 1986.

[28] S. Wang, Y. Wang, M. Jin, X. D. Gu, and D. Samaras. Conformal geometry and its applications on 3d shape matching, recognition, and stitching. *PAMI*, 29(7):1209 – 1220.

[29] Y. Wang, M.-C. Chiang, and P. M. Thompson. Mutual information-based 3d surface matching with applications to face recognition and brain mapping. *ICCV05*, I:527–534.

[30] Y. Wang, M. Gupta, S. Zhang, S. Wang, X. Gu, D. Samaras, and P. Huang. High resolution tracking of non-rigid 3d motion of densely sampled data using harmonic maps. *ICCV05*, I:388–395.

[31] J. Wyngaerd, L. Gool, R. Koch, and M. Proesmans. Invariant-based registration of surface patches. *ICCV99*, I:301–306.

[32] A. Yuille, P. Hallinan, and D. Cohen. Feature extraction from faces using deformable templates. *IJCV*, 8(2):99–111, 1992.

[33] D. Zhang and M. Hebert. Harmonic maps and their applications in surface matching. *CVPR99*, II:524–530.

[34] S. Zhang and P. Huang. High resolution, real time 3d shape acquisition. In *CVPR04 Workshop on Real-time 3D Sensors and Their Use*, pages 28–37.